

## Article

# PEDOT:PSS/PEDOT Film Chemiresistive Sensors for Hydrogen Peroxide Vapor Detection under Ambient Conditions

Xiaowen Xie <sup>1</sup>, Nan Gao <sup>2</sup>, Ling Zhu <sup>1</sup>, Matthew Hunter <sup>3</sup> , Shuai Chen <sup>1,2,\*</sup>  and Ling Zang <sup>3,\*</sup> 

<sup>1</sup> Jiangxi Key Laboratory of Flexible Electronics and School of Pharmacy, Jiangxi Science and Technology Normal University, Nanchang 330013, China

<sup>2</sup> Jiangxi Engineering Laboratory of Waterborne Coating, Nanchang 330013, China

<sup>3</sup> Nano Institute of Utah and Department of Materials Science and Engineering, University of Utah, Salt Lake City, UT 84112, USA

\* Correspondence: shuaichen@jxstnu.edu.cn (S.C.); lzang@eng.utah.edu (L.Z.);  
Tel.: +1-801-587-1551 (L.Z.); Fax: +1-801-581-4816 (L.Z.)

**Abstract:** Hydrogen peroxide (aqueous solution of H<sub>2</sub>O<sub>2</sub>) is one of the most used reagents in a medical sterilization, environmental disinfection, food storage, and other fields. However, hydrogen peroxide has the potential to cause serious harm to biological health and environmental safety. There are many methods (especially electrochemistry) for H<sub>2</sub>O<sub>2</sub> detection in liquid phase systems, but a lack of methods for vapor detection. This is due to its colorless and tasteless nature, as well as the oxidative activity of the molecule and its coexistence with humidity. In this study, poly(3,4-ethylenedioxythiophene):polystyrene sulfonate (PEDOT:PSS), one of the most commercially successful and widely used conductive polymers, was employed to fabricate an all-organic chemiresistive sensor for simple, real-time, and on-site sensing of hydrogen peroxide vapor (HPV) at room temperature. In comparison with pristine PEDOT:PSS film, the PEDOT:PSS/PEDOT film was prepared by in situ electrochemical polymerization. Upon exposure to different concentrations of HPV, it was found that the hydrophobic and porous PEDOT layer could weaken the interference of humidity in HPV sensing, resulting in a more sensitive and accurate response. At 1.0 ppm HPV concentration, the resistance signal response was increased by nearly 89% compared with the pristine PEDOT:PSS film. This PEDOT-film-based chemiresistive sensor showcases the possibility for further development of nonenzymatic HPV monitoring technology.

**Keywords:** PEDOT:PSS; PEDOT; conducting polymer; hydrogen peroxide; gas detection; chemosensor; chemiresistive sensor; film sensor



**Citation:** Xie, X.; Gao, N.; Zhu, L.; Hunter, M.; Chen, S.; Zang, L. PEDOT:PSS/PEDOT Film Chemiresistive Sensors for Hydrogen Peroxide Vapor Detection under Ambient Conditions. *Chemosensors* **2023**, *11*, 124. <https://doi.org/10.3390/chemosensors11020124>

Academic Editor: Masanori Ando

Received: 30 December 2022

Revised: 1 February 2023

Accepted: 6 February 2023

Published: 7 February 2023



**Copyright:** © 2023 by the authors. Licensee MDPI, Basel, Switzerland. This article is an open access article distributed under the terms and conditions of the Creative Commons Attribution (CC BY) license (<https://creativecommons.org/licenses/by/4.0/>).

## 1. Introduction

Hydrogen peroxide (the aqueous form of H<sub>2</sub>O<sub>2</sub>) is one of the most used reagents in medical sterilization, environmental disinfection, food storage, and other fields. The same properties that make it a useful chemical also give H<sub>2</sub>O<sub>2</sub> the potential to cause serious biological and environmental damage. Since the assertion of the Public Health Emergency of International Concern (PHEIC) following the discovery of the novel coronavirus (COVID-19), disinfection measures have been strengthened worldwide in public facilities, transportation, hospitals, wastewater treatment facilities, and in day-to-day living scenarios [1,2]. One method of improved disinfection is the vaporization of H<sub>2</sub>O<sub>2</sub>. Vaporized H<sub>2</sub>O<sub>2</sub> is colorless and tasteless and can achieve rapid and comprehensive diffusion on walls, ground, equipment, tables, chairs, and other surfaces for disinfecting against coronavirus. However, its strong oxidation can cause skin, eye, and mucous membrane corrosion and irritation, effects that are only exacerbated by the dramatic increase in H<sub>2</sub>O<sub>2</sub> consumption. Furthermore, H<sub>2</sub>O<sub>2</sub> in the body produces free radicals after oxidative reaction. These free radicals can result in cell damage and lesions, leading to respiratory and inflammatory diseases, and even some cancers. When its concentration is 3 wt.% or lower, it causes

gastrointestinal and eye irritation [3] and is deadly at a concentration of only 75 ppm [4]. The Industrial Hygiene Conference of the United States Government stipulates that the threshold value of H<sub>2</sub>O<sub>2</sub> is 1 ppm, and the short-term contact (15 min) limit is 2 ppm [5].

There are many detection methods for H<sub>2</sub>O<sub>2</sub> in liquid phase systems. The most common of these utilize colorimetric [6,7], electrochemical [8], enzymatic chemical [9], and fluorescence methods [10]. In contrast, there has been much less effort and success in the development of a simple, efficient sensor technology suitable for real-time detection of H<sub>2</sub>O<sub>2</sub> vapor (HPV). The critical challenge derives from its coexistence with humidity and oxidative activity in the vapor phase. The detection of HPV based on fluorescence and colorimetric signals has been reported [11–14]. Chemiresistive sensors are a more simple-to-use and accurate alternative to fluorescence and colorimetric sensors, and the electrical signal data acquired are far more quantitative than the latter [15]. As a result, chemiresistive sensors show promise for future commercialization.

Semiconducting metal oxides were often used as gas-sensing materials for chemiresistive detection. However, they must withstand high operating temperatures (usually 200–500 °C). For example, Aroutiounian et al. prepared Co-doped SnO<sub>2</sub> thin films [16] and La-doped ZnO thin films [17] that were able to detect up to 10 ppm HPV at temperatures of 200 °C and 240 °C, respectively. Carbon-based nanomaterials have good electrical properties, thermal properties, and high surface-to-volume ratio, as well as the capability to operate at lower temperatures than metal oxides. It can therefore be assumed that a carbon-nanomaterial-based chemiresistive sensor could achieve high sensitivity at relatively low temperatures. For example, Adamyan et al. [18] prepared multilayer carbon nanotubes coated with tin oxide nanoparticles (MWCNTs/SnO<sub>2</sub>) to detect HPV at an operating temperature of 100 °C. Verma et al. [19] developed a sensor based on a MWCNTs and metal-phthalocyanines (MPc) composite and was able to sense HPV at room temperature. Lee et al. [20] fabricated a nanocomposite sensor based on metalloporphyrin derivative (TiOTPPy) and platinum-nanoparticles-decorated single-walled carbon nanotube (SWCNTs) for room-temperature monitoring of HPV. While these systems were able to detect HPV at high and low temperatures, complicated design and fabrication of the composite material architecture, limited matching stability between different phases, and the involvement of noble metal catalysts will undermine the advantages of these systems.

Intrinsically conducting polymers (ICPs) are polymers with conjugated structures that can conduct electricity after electrochemical or chemical doping (oxidation) and are a foundation of chemosensor materials. Both the precursor monomer and the polymer film of ICPs have excellent electrochemical activity. This activity is highly tunable by controlling the electrochemical polymerization process. This makes ICPs especially suitable for detecting various analytes in liquid phase systems, such as metal cations, anions, and biomolecules [15]. Poly(3,4-ethylenedioxythiophene):polystyrene sulfonate (PEDOT:PSS, Figure 1a) is a widely used, commercially available ICP. It has been combined with other materials for the sensing of various gases (moisture, ammonia, CO, NO<sub>x</sub>, etc.) at room temperature, as well as the sensing of H<sub>2</sub>O<sub>2</sub> in liquid phase [21–24]. At present, our group has reviewed its application in electrochemical and electronic chemosensors [15]. In brief, the powerful composite and film processing ability, as well as adjustable and excellent electric properties, of PEDOT:PSS will provide great opportunities for its use in HPV detection, but the hygroscopicity of its dry film should be considered. High humidity greatly affects the functionality of all chemosensors. This is a critical application problem that the current sensor field has been committed to solve. Indeed, it has been reported by Naficy's group that PEDOT:PSS can be combined with horseradish peroxidase (HRP) to construct a chemiresistive HPV sensor [25]; however, the study neither discussed the interference effect of humidity nor fully considered the unfavorable factors such as enzyme stability and the compatibility issue between it with PEDOT:PSS, limiting its applicability. The oxidizing nature of HPV makes it easy to distinguish from other interference analytes due to a lack of interference from other gas phase components, so selectivity, except from the moisture, is generally not considered as a major factor in the study. However, if

chemically or biologically active substrates, such as HRP, are introduced into the gas-sensing materials, the influence of other components in the environment on the sensing materials and interference on the detection effect must be taken into account.

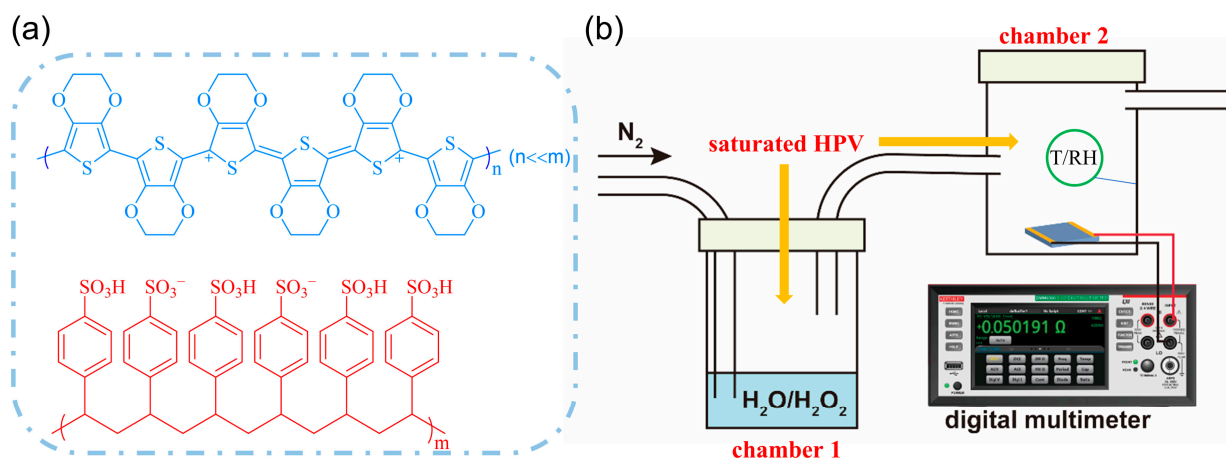


**Figure 1.** (a) Molecular structure of PEDOT:PSS. (b) Schematic diagram of HPV-sensing system.

Herein, we report a chemiresistive sensor based on PEDOT:PSS/PEDOT film to achieve direct detection of different concentrations of HPV. The hydrophobic, porous PEDOT layer was polymerized on the surface of PEDOT:PSS film by an electrochemical method. The resistance response of the composite film to different concentrations of HPV, the influence of moisture components on material stability and response accuracy, and the role of the PEDOT layer have been investigated and discussed in comparison with a single PEDOT:PSS system. This study verified the reliability of PEDOT-based ICPs as all-organic gas-sensing materials for HPV monitoring. Unlike other current systems, the presented materials did not rely on the addition of active enzymes such as HRP, metal-based and carbon-based inorganic gas-sensing materials, complex material micro-nano structure regulation, or architecture modification technology.

## 2. Materials and Methods

### 2.1. Materials

Aqueous dispersion of PEDOT:PSS was completed with Clevios™ PH1000 (1.0–1.3 wt.% solid content). In addition, 3,4-Ethylenedioxythiophene (EDOT, 97%) and all organic solvents were purchased from J&K Scientific Ltd. (Shanghai, China). Hydrogen peroxide (H<sub>2</sub>O<sub>2</sub> aqueous solution, 30 wt.%) was purchased from Fuchen (Tianjin) Chemical Reagent Co., Ltd (Tianjin, China). Tetrabutylammonium hexafluorophosphate (Bu<sub>4</sub>NPF<sub>6</sub>, 98%) was purchased from Shanghai Energy Chemical Co., Ltd. (Shanghai, China). Indium-tin-oxide-coated glass (ITO-glass, sheet resistance < 10 Ω sq<sup>-1</sup>) was purchased from Zhuhai Kaivo Optoelectronic Technology Co., Ltd. (Zhuhai, China). Ultra-pure water was all laboratory-made by an ultrapure water device (UPT-11-100T, Sichuan Ulupure Ultrapure Technology Co., Ltd. Sichuan, China).

### 2.2. Preparation of PEDOT-Based Composite Films

All PEDOT-based composite films in this work were deposited on pre-cut ITO substrates (1 cm × 2 cm). Before use, the ITO-glass substrates were prepared by ultrasonic cleaning and ultraviolet ozone cleaning. They were then washed with pure water, soaked in dichloromethane, acetone, ethanol, and pure water for 20 min, then blow-dried with high-purity N<sub>2</sub>. Finally, they were put into the ultraviolet ozone cleaning machine again with the ITO coating side up for 15 min treatment, and then stored in pure isopropanol solution and dried with pure N<sub>2</sub> before use. The PEDOT-based films in the following section were all completely covering the substrate.

**PEDOT:PSS film:** The ITO-glass was placed in the suction plate center of a spin coater, and 100  $\mu\text{L}$  PEDOT:PSS aqueous dispersion was dropped onto the glass surface until it was completely covered. The rotation speed was set at 1500 rpm for 30 s, then 2500 rpm for 20 s, and repeated three times. The film was then dried at 50  $^{\circ}\text{C}$  for 2 h in a drying oven.

**PEDOT:PSS/PEDOT film:** The PEDOT:PSS film coated on ITO-glass prepared above was selected as the working electrode, platinum (1.5 cm  $\times$  1.5 cm) was used as the counter electrode, and Ag/AgCl was used as the reference electrode. Relying on a three-electrode system, EDOT (1 mM) added into ACN-Bu<sub>4</sub>NPF<sub>6</sub> (0.1 M) electrolyte was electrochemically polymerized into a PEDOT:PSS/PEDOT film at room temperature. By regulating the amount of charge (10 mC, 20 mC, 30 mC) applied by the electrochemical chronopotentiometry technique, three films were achieved for comparison. They were then washed with acetonitrile and dried with N<sub>2</sub>.

### 2.3. Characterization

UV-Vis absorption spectra of all films were collected using a UV-Vis spectrophotometer (Specord Plus 200, Jena, Germany). Fourier-transform infrared (FT-IR) spectra were recorded on a Bruker Vertex 70 FT-IR spectrometer (PerkinElmer Co., Ltd., Shanghai, China). The polymerization of EDOT and the electrochemical properties of materials were measured on a three-electrode system using an electrochemical workstation (Versa STAT 3, Princeton Applied Research, Princeton, NJ, USA). The morphology and microstructural observations were characterized via a metallographic microscope (LW300LJT, Beijing Cewei Optoelectronic Technology Co., Ltd., Beijing, China) and scanning electron microscope (SEM, FEI-QUANTA250, Portland, ORE, USA). The surface hydrophobicity of films was determined by measuring the contact angle under ambient conditions (25  $\pm$  3  $^{\circ}\text{C}$  and 50% relative humidity (RH)) using a contact angle goniometer (SDC-100, Dongguan Shengding Precision Instrument Co., Ltd., Dongguan, China).

### 2.4. Construction of HPV Detection System

Similar to our and other groups' previously published methods [11–14,25] in terms of Manatt's report [26], 30 wt.% H<sub>2</sub>O<sub>2</sub> solution was diluted by different volumes of pure water into 3.5 wt.%, 1.4 wt.%, 0.7 wt.%, and 0.35 wt.% solutions and placed in a closed container (chamber 1, Figure 1b) for 12 h to produce different saturated (equilibrium) vapor pressures (10.5 ppm, 4.0 ppm, 1.9 ppm, and 1.0 ppm, respectively) of HPV. However, unlike the previous single chamber for optical sensing, in order to evaluate the sensing response of PEDOT-based composite films to HPV and help the vapor diffusion, while also avoiding the inferior effect of prolonged exposure on electrical signal pattern detection, a two-chamber test system was built as shown in Figure 1b, just like the setup reported by Naficy and co-workers [25]. In detail, the gas delivery of the system consisted of two connected chambers, each with an air inlet and an air outlet. The first chamber (200 mL, wrapped in foil to protect from light) was for HPV generation and stored 20 mL of H<sub>2</sub>O<sub>2</sub> standard solution with a certain concentration; the saturated HPV was loaded by slowly injecting N<sub>2</sub> (50 mL/min) into the solution and bubbling into chamber 2. Chamber 2 was for the HPV test, which was equipped with a hygrometer probe to monitor the ambient temperature and relative humidity (RH) during the test. The sensor film was fixed between the bottom and air inlet of chamber 2 to monitor the changes of incoming HPV concentrations after it reached the equilibrium state (staying 30 s after N<sub>2</sub>-flow beginning). The outlet of the second chamber was kept open during the test and led to an airtight anti-pour paraffin glass bubbler, whose outlet led to a sink by a conduit to ensure safety. The entire test device system was placed in a laboratory fume hood, maintaining a normal open space and room temperature (26  $\pm$  0.5  $^{\circ}\text{C}$ ) environment. In addition, due to their risk, all experiments were conducted in a non-sunlight environment during the daytime, in accordance with the safety management system of our laboratory.

The chemiresistive signal response of the PEDOT-based film to HPV was tested and recorded by a digital multimeter (DMM 6500 SourceMeter, Keithley, Beijing, China), which

can ensure real-time data collection. The data analysis was processed by computer software. The transmission of the resistance signal was carried out by two symmetrical copper conduction strips (0.2 cm × 7 cm, 0.7 cm apart) on the surface of the film and two external copper wires for instrument connection. In addition,  $\Delta R/R_0$  was defined as the resistance response of each film during testing, where  $\Delta R = R - R_0$ , and  $R_0$  is the resistance value measured at 25% RH.

### 3. Results and Discussion

#### 3.1. Chemiresistive HPV Sensing Based on PEDOT:PSS Film

PEDOT:PSS film has a distinct response to the concentration change of HPV. The time-dependent resistance curves of PEDOT:PSS films exposed to different concentrations of HPV (10.5 ppm, 4.0 ppm, 1.9 ppm, 1.0 ppm) are presented in Figure 2a. The film resistance gradually increases from the initial value (about 87  $\Omega$ ), maintains a peak resistance value for a period of time, and then gradually declines. The valley value after about 70 min exposure and the initial resistance are similar. The exposure of different concentrations of HPV also has a clear effect on the detection response of the film. With the decrease of HPV concentration, the resistance response values calculated from the first peak of the curve were 10.87 (10.5 ppm), 6.38 (4.0 ppm), 3.03 (1.9 ppm), and 0.38 (1.0 ppm), and the times to reach the first peak were 22 min, 24 min, 12 min, and 37 min, respectively. The overall trend showed a faster response and stronger signal contrast congruent with the increase of HPV concentrations. For example, the film required a long time to reach the first resistance peak at a low concentration of 1.0 ppm (Figure 2a, inset). The film resistance continued to rise slowly, from 40 min to 80 min. When the resistance reaches the first peak, it is found that there is a long period of resistance equilibrium stage for the concentrations of 1.9 ppm and 4.0 ppm, while the resistance value of the film under 10.5 ppm HPV continuously drops to about 200  $\Omega$ . These phenomena are closely related to the oxidative levels of PEDOT:PSS films at different HPV concentrations, and the influence of humidity accompanied the whole detection process. Nevertheless, for the response to 1.9 ppm HPV, the film resistance can reach the first peak (about four times that of the initial resistance value) within 12 min, meeting the requirement of the safety threshold (2.0 ppm, 15 min).

It was found that with the entry of HPV, the relative humidity gradually increased from the original 25% RH to 100% RH during real-time measurements taken in the second detection chamber. This is because HPV was generated from the H<sub>2</sub>O<sub>2</sub> aqueous solution. Therefore, the material must be able to function with a change of inherent moisture in the detection environment. This is replicative of how HPV would behave in an actual environment, considering the presence and changes in humidity. Although this is a serious problem faced by most gas phase sensors and is one of the critical issues for the developing HPV sensing technology, from another point of view, the presence and change of humidity is inevitable in the actual environment. The detection system constructed in this paper can fully reflect the occurrence and diffusion process and behavior of HPV in an actual environment. In addition, PEDOT:PSS itself has a large number of hydrophilic sulfonic acid groups and, thus, a strong moisture-absorbing capability, which provides a basis for its humidity-sensing applications [27,28]. The film's hygroscopicity will help its adsorption of HPV and ensure the impact of H<sub>2</sub>O<sub>2</sub> on the film's resistance signal response. To further explore and evaluate the effect of the moisture component in HPV on the PEDOT:PSS film, we replaced the H<sub>2</sub>O<sub>2</sub> aqueous solution in the first chamber with pure water. As seen in the resistance-time curve of PEDOT:PSS film shown in Figure 2b, under the continuous increase of ambient humidity, the resistance value of the film reaches its maximum value at about 50–60% RH (3.3 times of the initial value). It then decreases with an increase of humidity to the same level at about 30 min. At about 40 min (humidity reaches 100% RH), the resistance value is 0.59 times lower than the initial value. This behavior ascribed to the microstructure change of the PEDOT:PSS film, as evidenced by other researchers [27–29]. In general, PEDOT:PSS has a granular structure, in which PEDOT<sup>+</sup>-rich grains (conductive) are surrounded by PSS<sup>−</sup> chains (insulator, hydrophilic). When the polymer chains of

PSS<sup>-</sup> swell after moisture adsorption, the interconnections between conductive PEDOT<sup>+</sup> segments will be destroyed and then result in an increased electrical resistance. At the same time, ascribed to its strong dipole moment, the water molecules can screen the conductive sites located in the PEDOT<sup>+</sup>-rich regions, thus further weakening the film's conductivity [30]. If the chamber humidity further reached 60% RH, a water meniscus layer formed on the surface of the PEDOT:PSS film (Figure 2b, inset) due to the temporary saturation adsorption of moisture. Accordingly, a decrease of resistance was observed, which may be attributed to the partial dissolution of PSS<sup>-</sup> and the more opened electric channel of PEDOT<sup>+</sup> segments. For long-term moisture absorption or under high humidity, PEDOT:PSS film will present a hydrogel state, so it has stability in sensing applications with a reasonable detection time, and after water loss, it can partially restore the original dry film state.

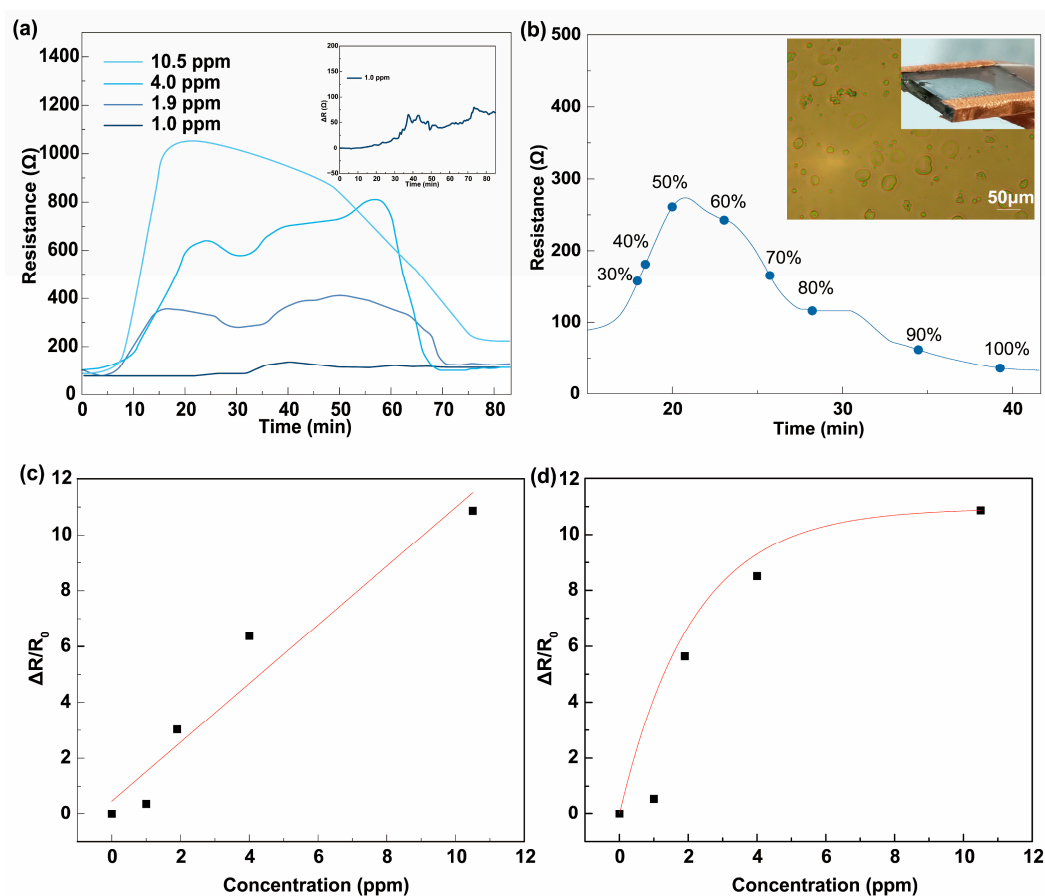


**Figure 2.** (a) Resistance-time curves of PEDOT:PSS films in different concentrations of HPV. Inset: resistance change-time curve of PEDOT:PSS film to 1.0 ppm HPV. (b) Resistance-time curve of PEDOT:PSS film under increasing ambient humidity (30% RH–100% RH), inset: optical microscope image of PEDOT:PSS film at high humidity, where the moisture could be condensed into droplets on the film surface. Resistance response-HPV concentration fitting curve of PEDOT:PSS films: (c)  $R$  = the first resistance peak, (d)  $R$  = the highest resistance peak.

As shown in Figure 2b, when the humidity in the second chamber has reached 100% RH at about 40 min, the surface resistance decreased due to the accumulation of some small water droplets on the film surface. In contrast, as shown in Figure 2a, the resistance still rose after 40 min. This means that in the HPV environment, at about 40 min, the moisture and oxidation doping of the H<sub>2</sub>O<sub>2</sub> component worked on the film resistance at the same time. Thus, the resistance response behavior of PEDOT:PSS films to HPV can be interpreted as a three-stage process. In the first stage, the film resistance rapidly increased to a peak value, which was due to the synergistic effect of the H<sub>2</sub>O<sub>2</sub> component and moisture

component. The moisture absorption of PSS<sup>-</sup> led to the decrease of inter-chain electrical interconnection of PEDOT<sup>+</sup>. At the same time, the electrons provided by the H<sub>2</sub>O<sub>2</sub> component also led to the hole loss of PEDOT<sup>+</sup> [25] and ultimately reduced the conductivity of the film. The second stage shows that the film resistance maintains a slight fluctuation at a certain level, which will neither increase significantly nor decrease significantly. On the one hand, continuous HPV access increased the humidity in the chamber to more than 50% RH, resulting in a decrease in film resistance. On the other hand, the H<sub>2</sub>O<sub>2</sub> component continued to lose the hole of PEDOT<sup>+</sup>, so that the conductivity of the film continuously decreased and the resistance increased. When entering the third stage, as HPV continued to enter, the moisture adsorbed on the film gradually increased, and finally the water droplets (visible to the naked eye) gathered on the film surface, resulting in a decrease in the film resistance. At this time, the water meniscus may also hinder its adsorption of HPV. The curve fitting of the resistance response ( $\Delta R/R_0$ ) data (Table 1) shows that when the peak value of the resistance reached in the first stage is selected as response data, the fitting curve ( $y = 0.4749 + 1.05071x$ , Figure 2c) is linear and the correlation coefficient is 0.93769. However, if the maximum value (not always the first peak value) of the film resistance is selected to calculate the response, the trend of the fitting curve ( $y = 1.77636 \times 10^{-5} + 10.94248 \times (1 - e^{(-x/2.11047)})$ ),  $R^2 = 0.84603$ , Figure 2d) proves the rationality of the three-stage process of the above inference. That is, there is indeed a role between the H<sub>2</sub>O<sub>2</sub> component of HPV and the film in the second stage.

**Table 1.** Comparison of resistance response ( $\Delta R/R_0$ ) of PEDOT:PSS and PEDOT:PSS/PEDOT films under different concentrations of HPV.

HPV (ppm)	PEDOT:PSS Film	PEDOT:PSS/PEDOT Film
1.0	0.54	0.72
1.9	5.64	5.98
4.0	8.51	13.82
10.5	10.87	17.73

In order to further evaluate the interaction mechanism between PEDOT:PSS and HPV, Raman (Figure 3a), FT-IR (Figure 3b), and UV-Vis absorption (Figure 3c) spectra of PEDOT:PSS films before and after the detection for different concentrations of HPV were obtained. The results show that after HPV detection, there were no particular variations in the Raman and FT-IR spectra. The UV-Vis absorption spectra changed to some extent, revealing that within the effective detection time and reasonable HPV concentration range, the molecular structure of PEDOT:PSS was stable [25], while the transparency and color of the film changed. Specifically, as shown in Figure 3a, in order to better reflect the stability of the PEDOT:PSS film itself in future practical-environment applications, we selected HPV with a concentration of 1.0 ppm, 10.5 ppm, and a maximum concentration of 100 ppm as the detection analytes. It can be seen that even at a concentration of 100 ppm, the spectral curve of the film after detecting HPV has no obvious changes in spectral type and peak shift compared with the original film. The peaks at 438 cm<sup>-1</sup>, 573 cm<sup>-1</sup>, and 990 cm<sup>-1</sup> represent the deformation of the oxyethylene ring caused by the presence of thiophene units in PEDOT<sup>+</sup>, and the peaks at 1257 cm<sup>-1</sup>, 1364 cm<sup>-1</sup>, and 1429 cm<sup>-1</sup> represent carbon-carbon intercylic bond stretching, carbon-infrared bond stretching, and symmetric stretching of the carbon double bond on the five-membered ring, respectively [31]. Similarly, in Figure 3b, no special changes in the infrared absorption peak intensity or peak shift of the PEDOT:PSS film before and after detection are found. The peak at 1137 cm<sup>-1</sup> represents the O-S stretching vibration, the peak at 1370 cm<sup>-1</sup> is the carbon-carbon intercylic bond of PEDOT<sup>+</sup>, and the peak at 1440 cm<sup>-1</sup> is the carbon-carbon double bond on the PEDOT<sup>+</sup> five-membered ring stretching vibrations [32]. As shown in Figure 3c, the absorption spectra of PEDOT:PSS films after the detection of different concentrations of HPV are different. Absorption at around 900 nm (corresponds to the bipolaron state of PEDOT<sup>+</sup>) in the near-infrared region decreases with increasing HPV concentration. In the PEDOT:PSS, the

concentration of bipolaron directly impacts the conductivity, where higher concentrations of bipolaron lead to higher conductivity [33]. The reduction in bipolaron concentration in the presence of more HPV, as suggested by UV–Vis spectra, agreed with the resistance data, in which the resistance increased with higher concentration of HPV. In addition, the decrease of the absorption peak at 500–600 nm (corresponding to the blue color of films) indicated that the color of the film is more transparent and less blue with the increase of HPV concentration.

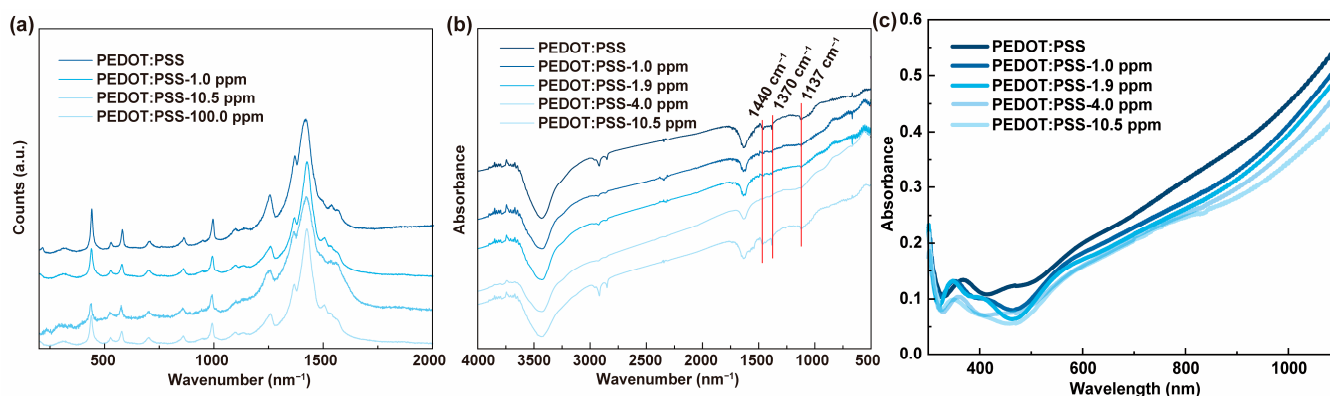


**Figure 3.** (a) Raman spectra, (b) Fourier transform infrared spectra, and (c) UV–Visible absorption spectra of PEDOT:PSS film before and after exposure to HPV with different concentrations.

### 3.2. Chemiresistive HPV Sensing Based on PEDOT:PSS/PEDOT Film

As discussed above, the presence of moisture components in HPV inevitably affects the resistance signal and stability of the PEDOT:PSS film, which may in turn affect the accuracy of detection. The hygroscopicity of PEDOT:PSS may contribute to its adsorption of the  $H_2O_2$  component in HPV at the first stage. In fact, the film's resistance response to HPV comes from the competitive effect of moisture and  $H_2O_2$  components. Some endeavors have been pursued to improve such issues. For example, Andò's group tried to add graphene to the surface of the PEDOT:PSS layer to resist the effects of moisture in  $CO_2$  detection [34]. On the other hand, the sensitivity and response speed could be improved by adjusting the microstructure and porosity of the gas-sensitive film. Constructing a composite system and controlling its structure and morphology is an effective way to improve the sensor response. The thin film structure of CPs polymerized by electrochemical methods may have a high porosity and can improve the adsorption capacity of gas molecules, which improves the sensor performance. The PEDOT:PSS film prepared by spin-coating on ITO-glass has a relatively smooth surface, meaning that it does not have high porosity to improve sensor performance. Electrochemical techniques may endow the polymerized film of ICPs with a high porosity to improve its adsorption capacity towards gaseous molecules. For example, Dunst et al. reported a pure PEDOT film with a cauliflower-like nanoparticle structure via electrochemical polymerization, which showed good sensing for  $NO_2$  gas [35]. Moreover, PEDOT itself can be seen as a hydrophobic polymer. Yang et al. realized the adjustment of hydrophilic and hydrophobic properties of PEDOT/alginate composite by adjusting the ratio between them during the in situ chemical oxidative polymerization of EDOT in the alginate matrix [36]. Thus, in this work, we would like to fabricate a PEDOT protective layer on the PEDOT:PSS film surface by electrochemical polymerization via a chronopotentiometry method. It is hoped that the PEDOT hydrophobicity of PEDOT could weaken the influence of moisture on the sensing film and HPV response and improve detection efficiency with the help of the high porosity of the PEDOT layer.

In order to explore the effect of the PEDOT layer on the hygroscopicity of PEDOT:PSS, three PEDOT:PSS/PEDOT films were prepared by controlling the charge amount of electrochemical polymerization of EDOT at 10 mC, 20 mC, and 30 mC. The water contact angles of these films were tested to evaluate the wettability of humidity or small water droplets formed by moisture during HPV testing on their surfaces. As shown in Figure 4,

when contacting with the smooth and hydrophilic PEDOT:PSS film surface, the water droplet spread rapidly, and the water contact angle was  $33^\circ$ . When the surface was covered with PEDOT and with the increasing of its thickness, the water contact angles increased significantly from  $57^\circ$ ,  $79^\circ$ , and  $104^\circ$ , respectively. In addition, the increase of water contact angle of the composite film may be partly in relation to the surface roughness change. Obviously, the porous surface of PEDOT:PSS/PEDOT (30 mC) film is composed of worm-like PEDOT structures, quite different from the smooth morphology of PEDOT:PSS (Figure 5). This is in line with our previous expectation that the PEDOT deposition could reduce the surface wettability of PEDOT:PSS film and create a porous surface, which may help to improve the film stability and anti-moisture interference as well as analyte adsorption during HPV detection.



**Figure 4.** Images of water contact angle test of composite films (PEDOT:PSS, PEDOT:PSS/PEDOT under different electrosynthetic charge amounts).

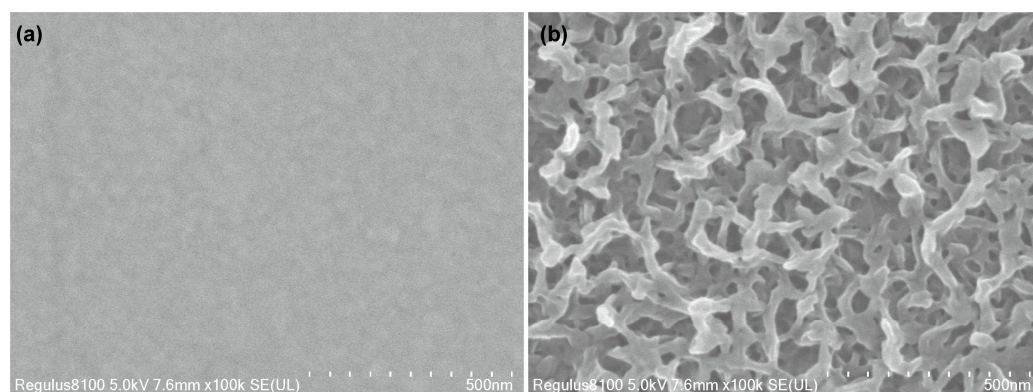


**Figure 5.** SEM images of (a) PEDOT:PSS film and (b) PEDOT:PSS/PEDOT (30 mC) film.

To explore the effect of the PEDOT coating on the sensing behavior of the composite film, similar to the above-mentioned PEDOT:PSS system, we first investigated the resistance-time curves of PEDOT:PSS/PEDOT films under the continuous increase of environmental humidity. As shown in Figure 6a, the resistance signal response of the films to humidity decreased with the increase of PEDOT on PEDOT:PSS surface. The initial resistance value of PEDOT:PSS film (about  $87 \Omega$ ) decreased from about  $80 \Omega$  (10 mC),  $61 \Omega$  (20 mC), to  $58 \Omega$  (30 mC) with the increase of the electrosynthetic charge amount of PEDOT from 10 mC and 20 mC to 30 mC, respectively. With the increase of humidity, the resistance trends of PEDOT:PSS/PEDOT (10 mC) and PEDOT:PSS/PEDOT (20 mC) film were similar to the PEDOT:PSS film. The resistance value peaks appeared at around 50–60% RH, about 6.0 and 2.0 times the initial value, respectively, and then continued to decline to the initial value level with the increase of humidity. By analyzing the response of these films to moisture by the peak value of the resistance curves, it is found that the humidity response weakened significantly with the increase of electrosynthetic charge amounts (i.e., thickness) of PEDOT. More promisingly, the resistance change of PEDOT:PSS/PEDOT (30 mC) film was less than  $\pm 10 \Omega$  when the humidity continued to increase to 100% RH, showing improved resistance to humidity interference (Figure 6b). Therefore, PEDOT:PSS/PEDOT (30 mC) film was used for the following HPV detection.

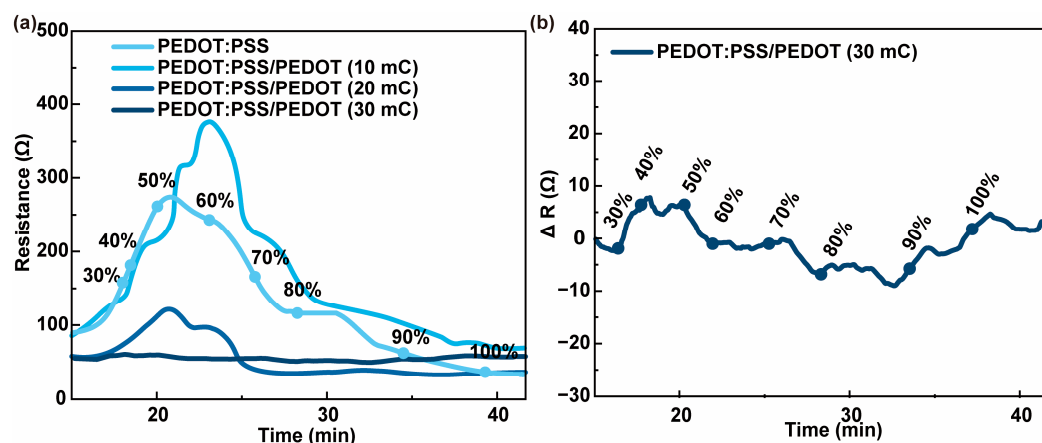


**Figure 6.** (a) Resistance-time curve of PEDOT:PSS and PEDOT:PSS/PEDOT films and (b) resistance change-time curve of PEDOT:PSS/PEDOT (30 mC) film under increased ambient humidity (30% RH~100% RH).

The resistance response of PEDOT:PSS/PEDOT (30 mC) films to different concentrations (10.5 ppm, 4.0 ppm, 1.9 ppm, 1.0 ppm) of HPV is shown in Figure 7a. The initial film resistance (60 Ω) increased rapidly after exposure to HPV before reaching a peak value and showed a faster response with the increase of HPV concentrations, even at 1.0 ppm. At the same HPV concentration, the film took a relatively short time to reach the first peak value compared to PEDOT:PSS (Figure 2a). Taking an HPV concentration of 4.0 ppm as an example, the PEDOT:PSS/PEDOT film reached peak resistance at about 17 min, while the PEDOT:PSS film took about 24 min (the highest peak was at ca. 57 min) and decreased by nearly 29%. The resistance response data (Table 1) were calculated by the maximum peak of the curves in Figure 7a, which showed a higher response than PEDOT:PSS film. Taking 10.5 ppm HPV as an example, the resistance response of PEDOT:PSS/PEDOT (30 mC) film was 17.73, which was 1.63 times higher than that of PEDOT:PSS film. However, for the low HPV concentration of 1.0 ppm, the film resistance value increased continuously with the detection time within 50 min (Figure 7b), so the resistance response was calculated using the highest data reached within 50 min, which was 1.33 times better than that of PEDOT:PSS film. These results may be ascribed to the porous structure of the PEDOT layer in the composite film, which is beneficial to the rapid vapor diffusion inside the sensing material, and its larger specific surface area provides stronger adsorption capacity to HPV. However, with the extension of exposure time to HPV, the resistance of PEDOT:PSS/PEDOT film decreased rapidly after reaching the peak. This means that although it is under the protection of PEDOT, the hygroscopicity of PEDOT:PSS will also inevitably interfere with its sensing response. Using the ExpAssoc function ( $y = 18.02388(1 - e^{(-x/2.55084)})$ ,  $R^2 = 0.8449$ ) to fit the resistance response-HPV concentration data, the fitted curve can be seen in Figure 7c.

To further clarify the effect of PEDOT composite on the resistance response of PEDOT:PSS film towards HPV, we also employed the same three-electrode electrochemical system to deposit single PEDOT film on ITO-glass surface. The amount of electrical charge applied during the chronopotentiometrical electropolymerization was 30 mC. As seen in the resistance-time change curve shown in Figure 8a, after exposure to different concentrations of HPV, PEDOT films also showed a pronounced resistance response. However, within the same duration time (50 min), the resistance values of PEDOT film continued to increase with the extension of exposure time from its initial value of about 48 Ω. The resistance value change of PEDOT film were narrowing along with decreased HPV concentration. At 1.0 ppm, the resistance of PEDOT film only increased by about 21% within 50 min (Figure 8b), whereas the first peak resistance of the PEDOT:PSS film increased by about 38%, and the PEDOT:PSS/PEDOT film increased by nearly 72% within 50 min compared with their initial resistance values. Thus, it can be reconfirmed that the hygroscopic PE-

DOT:PSS will inevitably interfere with its sensing response to HPV, and the recombination of PEDOT helps to shield the adverse effects of moisture.

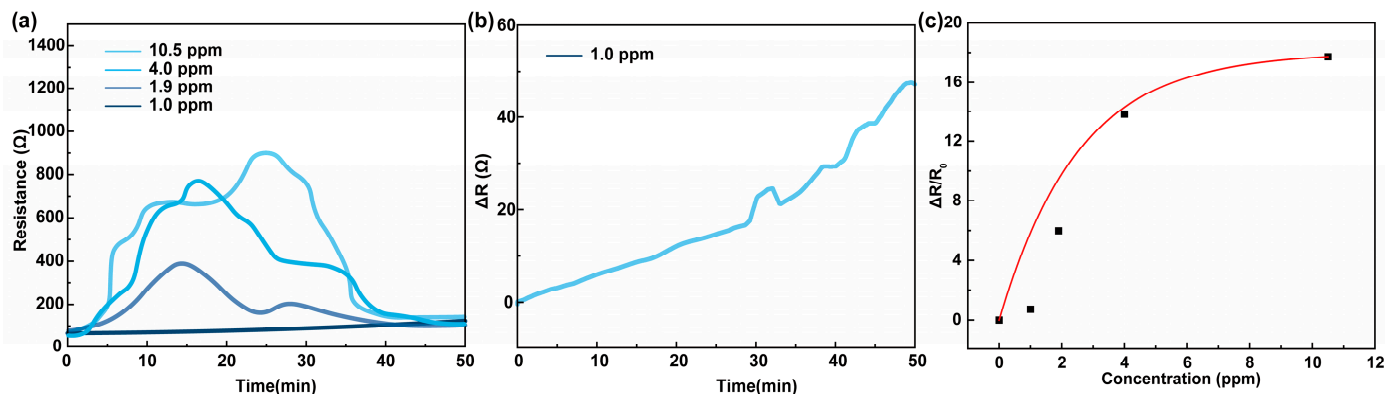


**Figure 7.** (a) Resistance-time curve to different concentrations of HPV, (b) resistance change-time curve to 1.0 ppm HPV and (c) resistance response-HPV concentration fitting curve of PEDOT:PSS/PEDOT (30 mC) film.

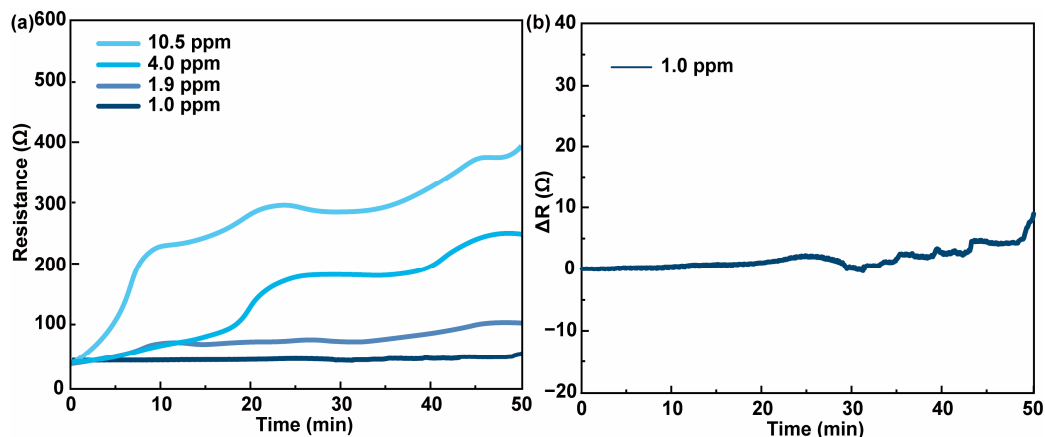


**Figure 8.** (a) Resistance-time curve of PEDOT film towards different concentrations of HPV and (b) resistance change-time curve of PEDOT film to 1.0 ppm HPV.

In summary, the resistance response curves of PEDOT:PSS film (Figure 2a) and PEDOT:PSS/PEDOT film (Figure 7a) in an HPV environment presented in three stages. First, a sharp rise with exposure time, which dropped at the peak before reaching a relative equilibrium, and finally dropped down to the level comparable to their initial values. According to the resistance response to humidity and the surface wettability test, as well as the response result of pure PEDOT film to HPV in Figure 8, the sensing behavior of PEDOT:PSS/PEDOT film in a 10.5 ppm, 4.0 ppm, and 1.9 ppm HPV environment can be divided into three stages accordingly. The first stage was that before the response resistance reached the highest peak value; the porous structure of the film surface made it quickly adsorb HPV. By consuming the holes in PEDOT<sup>+</sup>, the conductivity of the film decreased, and the resistance increased. At the same time, the moisture component in HPV began to condense into tiny water droplets on the hydrophobic surface, which can be considered as the Cassie state of a droplet. However, with the extension of exposure time, the water droplets on the surface of the film will absorb more moisture and their gravitational potential energy on the surface increased continuously. When it overcame the energy barrier between the Cassie and the Wenzel states, the Cassie-to-Wenzel transition will be achieved [37,38]. This process corresponds to the second stage, that is, the turning point before the rapid decrease of the films resistance after reaching the maximum value. Then at the third stage, the liquid droplets will further saturate the porous PEDOT layer and contact with the PEDOT:PSS layer. At this time, the film resistance decreased rapidly due to the emergence of ionic

conductivity, similar to the state of water meniscus on the surface of PEDOT:PSS film [30]. For 1.0 ppm HPV, the adsorption and response of PEDOT:PSS/PEDOT film to HPV will be in an unsaturated state within a limited detection time (Figure 8b). Thus, the transition process of HPV adsorption on the film surface from Cassie state to Wenzel state was slow, and the interaction between the film and H<sub>2</sub>O<sub>2</sub> component was also slow. As a result, the resistance increased continuously with prolonged time, as shown in Figure 7b, similar to PEDOT and PEDOT:PSS film but with a higher response.

#### 4. Conclusions

In this paper, through the method of quantitative electrochemical deposition, PEDOT:PSS/PEDOT film was prepared on the basis of PEDOT:PSS film electrode and was successfully used for the chemiresistive sensing of HPV. The interference from coexisting moisture and the positive effect of the hydrophobicity and porous structure of the PEDOT layer on the resistance response behavior of sensor films towards different concentrations of HPV were explored. The changes of its structure and morphology and the HPV detection mechanism were also studied by SEM, water contact angle, as well as Raman, FT-IR, and UV-Visible absorption spectra. The structural stability and reliability of PEDOT-film-based sensor for HPV detection were verified through the comparative study with PEDOT:PSS and PEDOT film. This is the first time that PEDOT-based ICPs have been used as gas-sensitive materials for chemiresistive detection of HPV. Further optimization of the composite material system to bring about a multi-mode detection concept may provide promising results to support the practical use of PEDOT-film-based chemiresistive sensors for developing real-time, portable, and miniaturized HPV sensor devices for monitoring much more chemically active vapor analytes. In addition, the design and development of more reliable generation and detection systems for synbiotic gas mixtures, such as moisture-H<sub>2</sub>O<sub>2</sub>, require further endeavors.

**Author Contributions:** Conceptualization, S.C.; methodology, S.C. and N.G.; software, N.G. and X.X.; validation, S.C. and N.G.; formal analysis, L.Z. (Ling Zhu) and X.X.; investigation, N.G. and S.C.; resources, N.G. and S.C.; data curation, X.X. and N.G.; writing—original draft preparation, S.C. and X.X.; writing—review and editing, S.C., M.H. and L.Z. (Ling Zang); supervision, S.C. and L.Z. (Ling Zang); funding acquisition, S.C. The submitted paper is the original work of the authors and has not been previously published, nor is not considered for publication anywhere else. All authors have read and agreed to the published version of the manuscript.

**Funding:** This research was funded by the Academic Development Project of TongXin Funds (grant number 2022161804).

**Institutional Review Board Statement:** Not applicable.

**Informed Consent Statement:** Not applicable.

**Data Availability Statement:** Not applicable.

**Conflicts of Interest:** The authors declare no conflict of interest.

#### References

1. Berger, D.; Gundermann, G.; Sinha, A.; Moroi, M.; Goyal, N.; Tsai, A. Review of aerosolized hydrogen peroxide, vaporized hydrogen peroxide, and hydrogen peroxide gas plasma in the decontamination of filtering facepiece respirators. *Am. J. Infect. Control* **2022**, *50*, 203–213. [[CrossRef](#)] [[PubMed](#)]
2. Dewey, H.M.; Jones, J.M.; Keating, M.R.; Budhathoki-Uprety, J. Increased use of disinfectants during the COVID-19 pandemic and its potential impacts on health and safety. *ACS Chem. Health Saf.* **2022**, *29*, 27–38. [[CrossRef](#)]
3. Holm, S.M.; Leonard, V.; Durrani, T.; Miller, M.D. Do we know how best to disinfect child care sites in the United States? A review of available disinfectant efficacy data and health risks of the major disinfectant classes. *Am. J. Infect. Control* **2019**, *47*, 82–91. [[CrossRef](#)]
4. Mucci, N.; Dugheri, S.; Bonari, A.; Farioli, A.; Rapisarda, V.; Garzaro, G.; Cappelli, G.; Arcangeli, G. Health risk assessment related to hydrogen peroxide presence in the workplace atmosphere-analytical methods evaluation for an innovative monitoring protocol. *Int. J. Occup. Med. Environ. Health* **2020**, *33*, 137–150. [[CrossRef](#)] [[PubMed](#)]

5. Reisert, S.; Schneider, B.; Geissler, H.; Van Gompel, M.; Wagner, P.; Schöning, M.J. Multi-sensor chip for the investigation of different types of metal oxides for the detection of H<sub>2</sub>O<sub>2</sub> in the ppm range. *Phys. Status Solidi A Appl. Mater. Sci.* **2013**, *210*, 898–904. [[CrossRef](#)]
6. Nguyen, N.D.; Van Nguyen, T.; Chu, A.D.; Tran, H.V.; Tran, L.T.; Huynh, C.D. A label-free colorimetric sensor based on silver nanoparticles directed to hydrogen peroxide and glucose. *Arab. J. Chem.* **2017**, *11*, 1134–1143. [[CrossRef](#)]
7. Liu, Q.; Chen, P.; Xu, Z.; Chen, M.; Ding, Y.; Yue, K.; Xu, J. A facile strategy to prepare porphyrin functionalized ZnS nanoparticles and their peroxidase-like catalytic activity for colorimetric sensor of hydrogen peroxide and glucose. *Sens. Actuators B* **2017**, *251*, 339–348. [[CrossRef](#)]
8. Siao, H.W.; Chen, S.M.; Lin, K.C. Electrochemical study of PEDOT-PSS-MDB-modified electrode and its electrocatalytic sensing of hydrogen peroxide. *J. Solid State Electrochem.* **2010**, *15*, 1121–1128. [[CrossRef](#)]
9. Xu, J.; Peng, R.; Ran, Q.; Xian, Y.; Tian, Y.; Jin, L. A highly soluble poly(3,4-ethylenedioxythiophene)-poly(styrene sulfonic acid)/Au nanocomposite for horseradish peroxidase immobilization and biosensing. *Talanta* **2010**, *82*, 1511–1515. [[CrossRef](#)]
10. Moßhammer, M.; Kühn, M.; Koren, K. Possibilities and challenges for quantitative optical sensing of hydrogen peroxide. *Chemosensors* **2017**, *5*, 28. [[CrossRef](#)]
11. Xu, M.; Bunes, B.R.; Zang, L. Paper-based vapor detection of hydrogen peroxide: Colorimetric sensing with tunable interface. *ACS Appl. Mater. Interfaces* **2011**, *3*, 642–647. [[CrossRef](#)]
12. Xu, M.; Han, J.M.; Zhang, Y.Q.; Yang, X.M.; Zang, L. A selective fluorescence turn-on sensor for trace vapor detection of hydrogen peroxide. *Chem. Commun.* **2013**, *49*, 11779–11781. [[CrossRef](#)]
13. Xu, M.; Han, J.M.; Wang, C.; Yang, X.M.; Pei, J.; Zang, L. Fluorescence ratiometric sensor for trace vapor detection of hydrogen peroxide. *ACS Appl. Mater. Interfaces* **2014**, *6*, 8708–8714. [[CrossRef](#)]
14. Chen, Q.Q.; Yang, L.; Guo, K.K.; Yang, J.L.; Han, J.M. Expedite fluorescent sensor prototype for hydrogen peroxide detection with long-life test substrates. *ACS Omega* **2021**, *6*, 11447–11457. [[CrossRef](#)]
15. Gao, N.; Yu, J.Y.; Tian, Q.Y.; Shi, J.; Zhang, M.; Chen, S.; Zang, L. Application of PEDOT:PSS and its composites in electrochemical and electronic chemosensors. *Chemosensors* **2021**, *9*, 79. [[CrossRef](#)]
16. Aroutiounian, V.; Arakelyan, V.; Aleksanyan, M.; Shahnazaryan, G.; Kacer, P.; Picha, P.; Kovarik, J.; Pekarek, J.; Joost, B. Thin-film SnO<sub>2</sub> and ZnO detectors of hydrogen peroxide vapors. *J. Sens. Sens. Syst.* **2018**, *7*, 281–288. [[CrossRef](#)]
17. Shahkhatuni, G.H.; Aroutiounian, V.M.; Arakelyan, V.M.; Aleksanyan, M.S.; Shahnazaryan, G.E. Investigation of sensor made of ZnO:La for detection of hydrogen peroxide vapours by impedance spectroscopy method. *J. Contemp. Phys. Armen. Acad. Sci.* **2019**, *54*, 188–195. [[CrossRef](#)]
18. Adamyan, Z.N.; Sayunts, A.G.; Khachaturyan, E.A.; Araqelyan, V.M.; Aroutiounian, V.M.; Joost, B. Study of hydrogen peroxide vapors sensors based on carbon nanotubes coated with tin oxide nanoparticles. *J. Contemp. Phys. Armen. Acad. Sci.* **2019**, *54*, 57–64. [[CrossRef](#)]
19. Verma, A.L.; Saxena, S.; Saini, G.S.S.; Gaur, V.; Jain, V.K. Hydrogen peroxide vapor sensor using metal-phthalocyanine functionalized carbon nanotubes. *Thin Solid Film.* **2011**, *519*, 8144–8148. [[CrossRef](#)]
20. Lee, D.J.; Choi, S.W.; Byun, Y.T. Room temperature monitoring of hydrogen peroxide vapor using platinum nanoparticles-decorated single-walled carbon nanotube networks. *Sens. Actuators B Chem.* **2018**, *256*, 744–750. [[CrossRef](#)]
21. Hasani, A.; Dehsari, H.S.; Gavgani, J.N.; Shalamzari, E.K.; Salehi, A.; Afshar Taromi, F.; Mahyari, M. Sensor for volatile organic compounds using an interdigitated gold electrode modified with a nanocomposite made from poly(3,4-ethylenedioxythiophene)-poly(styrenesulfonate) and ultra-large graphene oxide. *Microchim. Acta* **2015**, *182*, 1551–1559. [[CrossRef](#)]
22. Shinde, S.; Jiang, C.Y.; Zheng, C.X.; Wang, Y.Z.; Lin, K.M.; Koinkar, P.M. Room-temperature and flexible PEDOT:PSS-WO<sub>3</sub> gas sensor for nitrogen dioxide detection. *Mod. Phys. Lett. B* **2019**, *33*, 1940013. [[CrossRef](#)]
23. Tang, L.; Wu, S.; Qu, J.; Gong, L.; Tang, J. A review of conductive hydrogel used in flexible strain sensor. *Materials* **2020**, *13*, 3947. [[CrossRef](#)] [[PubMed](#)]
24. Rahimzadeh, Z.; Naghib, S.M.; Zare, Y.; Rhee, K.Y. An overview on the synthesis and recent applications of conducting poly(3,4-ethylenedioxythiophene) (PEDOT) in industry and biomedicine. *J. Mater. Sci.* **2020**, *55*, 7575–7611. [[CrossRef](#)]
25. Giaretta, J.E.; Oveissi, F.; Dehghani, F.; Naficy, S. Paper-based, chemiresistive sensor for hydrogen peroxide detection. *Adv. Mater. Technol.* **2021**, *6*, 2001148. [[CrossRef](#)]
26. Manatt, S.L.; Manatt, M.R.R. On the analyses of mixture vapor pressure data: The hydrogen peroxide/water system and its excess thermodynamic functions. *Chem. A Eur. J.* **2004**, *10*, 6540–6557. [[CrossRef](#)]
27. Taccola, S.; Greco, F.; Zucca, A.; Innocenti, C.; Fernández, C.D.J.; Campo, G.; Sangregorio, C.; Mazzolai, B.; Mattoli, V. Characterization of free-standing PEDOT:PSS/iron oxide nanoparticle composite thin films and application as conformable humidity sensors. *ACS Appl. Mater. Interfaces* **2013**, *5*, 6324–6332. [[CrossRef](#)]
28. Aziz, S.; Chang, D.E.; Doh, Y.H.; Kang, C.U.; Choi, K.H. Humidity sensor based on PEDOT:PSS and zinc stannate nano-composite. *J. Electron. Mater.* **2015**, *44*, 3992–3999. [[CrossRef](#)]
29. Romero, F.J.; Rivadeneyra, A.; Becherer, M.; Morales, D.P.; Rodríguez, N. Fabrication and characterization of humidity sensors based on graphene oxide-PEDOT:PSS composites on a flexible substrate. *Micromachines* **2020**, *11*, 148. [[CrossRef](#)]
30. Popov, V.I.; Kotin, I.A.; Nebogatikova, N.A.; Smagulova, S.A.; Antonova, I.V. Graphene-PEDOT:PSS humidity sensors for high sensitive, low-cost, highly-reliable, flexible, and printed electronics. *Materials* **2019**, *12*, 3477. [[CrossRef](#)]

31. Sakamoto, S.; Okumura, M.; Zhao, Z.; Furukawa, Y. Raman spectral changes of PEDOT-PSS in polymer light-emitting diodes upon operation. *Chem. Phys. Lett.* **2005**, *412*, 395–398. [[CrossRef](#)]
32. Bhowal, A.C.; Talukdar, H.; Kundu, S. Preparation, characterization and electrical behaviors of PEDOT:PSS-Au/Ag nanocomposite thin films: An ecofriendly approach. *Polym. Bull.* **2019**, *76*, 5233–5251. [[CrossRef](#)]
33. Yan, Y.; Yang, G.; Xu, J.L.; Zhang, M.; Kuo, C.C.; Wang, S.D. Conducting polymer-inorganic nanocomposite-based gas sensors: A review. *Sci. Technol. Adv. Mater.* **2021**, *21*, 768–786. [[CrossRef](#)]
34. Andò, B.; Baglio, S.; Di Pasquale, G.; Pollicino, A.; Graziani, S.; Gugliuzzo, C.; Lombardo, C.; Marletta, V. Direct printing of a multi-layer sensor on pet substrate for CO<sub>2</sub> detection. *Energies* **2019**, *12*, 557. [[CrossRef](#)]
35. Dunst, K.; Karczewski, J.; Jasiński, P. Nitrogen dioxide sensing properties of PEDOT polymer films. *Sens. Actuators B Chem.* **2017**, *247*, 108–113. [[CrossRef](#)]
36. Yang, B.G.; Yao, F.L.; Ye, L.; Hao, T.; Zhang, Y.B.; Zhang, L.; Dong, D.Y.; Fang, W.C.; Wang, Y.; Zhang, X.Y.; et al. A conductive PEDOT/alginate porous scaffold as a platform to modulate the biological behaviors of brown adipose-derived stem cells. *Biomater. Sci.* **2020**, *8*, 3173–3185. [[CrossRef](#)]
37. Pendyala, P.; Kim, H.N.; Grewal, H.S.; Chae, U.; Yang, S.; Cho, I.J.; Song, S.; Yoon, E.S. Internal-flow-mediated, tunable one-dimensional Cassie-to-Wenzel wetting transition on superhydrophobic microcavity surfaces during evaporation. *Nanoscale Microscale Thermophys. Eng.* **2019**, *23*, 275–288. [[CrossRef](#)]
38. Azimi, A.; He, P. Effect of gravity in the Cassie-to-Wenzel transition on a micropatterned surface. *MRS Commun.* **2020**, *10*, 129–134. [[CrossRef](#)]

**Disclaimer/Publisher’s Note:** The statements, opinions and data contained in all publications are solely those of the individual author(s) and contributor(s) and not of MDPI and/or the editor(s). MDPI and/or the editor(s) disclaim responsibility for any injury to people or property resulting from any ideas, methods, instructions or products referred to in the content.